Acta Crystallographica Section B
Structural Science
ISSN 0108-7681

Five varieties of hydrogen bond in 1-formyl-3-thiosemicarbazide: an electron density study

Parthapratim Munshi,[a] Tejender S. Thakur,[b] Tayur N. Guru Row[a]* and Gautam R. Desiraju[b]*

[a]Solid State and Structural Chemistry Unit, Indian Institute of Science, Bangalore 560012, India, and [b]School of Chemistry, University of Hyderabad, Hyderabad 500046, India

Correspondence e-mail: ssctng@sscu.iisc.ernet.in, gautam_desiraju@yahoo.com

Received 29 April 2005
Accepted 18 October 2005

In an attempt to investigate the putative S—H···N hydrogen bond, we have studied the title compound, 1-formyl-3-thiosemicarbazide, which was revealed in a CSD search as a crystal structure which might show such an interaction. However, a redetermination of the structure at room temperature and careful analysis showed that the earlier study [Saxena *et al.* (1991). *Acta Cryst.* C**47**, 2374–2376] on which the CSD search was based was in error and that the possibility of an S—H···N hydrogen bond is negated. The presence of five other varieties of hydrogen bond (N—H···O, N—H···S, N—H···N, C—H···O, C—H···S) in the crystal packing prompted us to redirect our efforts and to undertake a study of the charge-density distribution at 90 K. The topological analysis of these five varieties of hydrogen bond was carried out with Bader's quantum theory of 'atoms in molecules' and by applying Koch–Popelier's criteria. The analysis reveals that the hydrogen-bond strength is highest for N—H···O and lowest for C—H···S with N—H···S, N—H···N and C—H···O forming the middle order.

1. Introduction

Hydrogen bonds (bridges) with sulfur as the donor (S—H) are not well studied and lie at the borderline between strong and weak interactions (Desiraju & Steiner, 1999). Owing to the fact that the electronegativity of the S atom (2.5) is much less than that of the O atom (3.5), the S—H group is a significantly weaker donor than the O—H group. Therefore, S—H···X (X = O, N, S, π) hydrogen bonds seem to occur in crystals very rarely, even in compounds that contain the pertinent functionalities. A recent study (Jetti *et al.*, 2004) indicates that in 4-aminothiophenol, what exists in the solid and liquid states is not the expected S—H···N hydrogen bond, but rather an ionic variant, N^+—H···S^-, that is obtained after proton transfer across the bridge. We have shown that such proton transfer is a favoured process. The question now arises as to how common the neutral S—H···N bond really is?

The putative S—H···N interaction is undoubtedly weak. We carried out computations on the H_2S–NH_3 and thiophenol–aniline systems and concluded that this interaction has a stabilization energy of around −12.6 kJ mol^{-1} (Spartan, RHF/6-31G**, −14.7 kJ mol^{-1}; GAMESS, RHF/6-31G**, −11.7 kJ mol^{-1} after BSSE correction) with an S···N distance (D) range of 3.60–4.00 Å. Clear cases of S—H···N hydrogen bonding are not to be found in the crystallographic literature.

A search of the Cambridge Structural Database (CSD; Allen, 2002; Allen & Motherwell, 2002) revealed only four hits that could possibly correspond to S—H···N interactions. All four cases are equivocal and perhaps S—H···N bonds appear as contacts imposed by the accompanying stronger interactions. In the first compound, 2,5-dimercaptothiadiazole (DMCTDZ), studied by Bats (1976), there is an appropriate S···N geometry but, in a perceptive analysis, the author had expressed doubt as to whether the H atom is bonded to the S atom or to the N atom. In the second compound 4,4′-diamino-2,2′,6,6′-tetramercaptobiphenyl (HIPMUO), there are two S···N contacts. In the shorter one (D, 3.40 Å), the S—H group is disordered. The longer one (3.84 Å) might correspond to a weak S—H···N interaction (Zhu-Ohlbach *et al.*, 1998). In the third compound (Ambalalavanan *et al.*, 2003), 3-(*p*-tolyl)-4-amino-5-mercapto-1,2,4-triazole (ILOQEF), the R factor is perhaps high (0.066) and there is a possibility of tautomerism so that instead of an S—H···N bond, an N—H···S bond could be formed instead. In the last compound, 1-formyl-3-thiosemicarbazide (SOJNAG; Saxena *et al.*, 1991), a possible S—H···N interaction (3.67 Å, 2.63 Å, 143°) was identified in the CSD search, although the accepted structural formula does not contain an S—H group.

To fully assess the viability of the S—H···N hydrogen bond in crystals, we have initiated a more detailed study of the four above-mentioned compounds. Here, we report our results on 1-formyl-3-thiosemicarbazide [see (I), *C*] from X-ray data collected at room temperature (293 K) and low temperatures (100 and 90 K), and an analysis of charge-density distributions obtained both from experimental data at 90 K and theoretical calculations with periodic boundary conditions. Subsequent papers will discuss the three other compounds. The molecular diagrams, shown in *A* and *B* in (I), are described in §3.

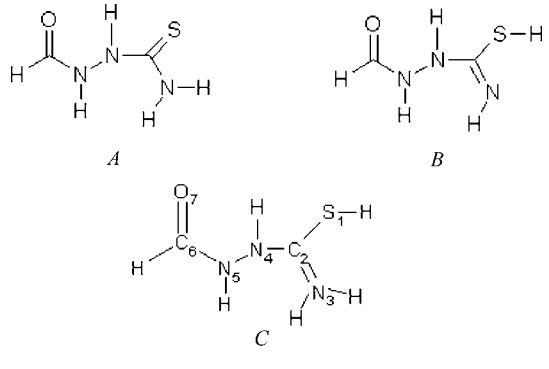

(I)

Analysis of charge density in a molecular crystal can be obtained from high-resolution X-ray diffraction data at low temperatures (Coppens, 1998). Chemical interactions can be characterized in terms of the deformation densities (Coppens, 1997; Koritsanszky & Coppens, 2001), using the Hansen and Coppens formalism (Hansen & Coppens, 1978), where the individual atomic densities are divided into three components, the core, a spherical expansion and contraction term (κ) for the valence shell, and the valence deformation, which is described in terms of density-normalized spherical harmonics ($d_{lm\pm}$), together with the corresponding radial expansion and contraction (κ') of the valence shell as given below

$$\rho_{\rm at}(\mathbf{r}) = \rho_{\rm core}(\mathbf{r}) + P_v\kappa^3\rho_{\rm val}(\kappa\mathbf{r}) + \sum_{l=0}^{l_{\rm max}} \kappa'^3 R_l(\kappa'\mathbf{r}) \sum_{m=0}^{l} P_{lm\pm} d_{lm\pm}(\vartheta, \varphi).$$

The density functions, also referred to as *multipoles*, are the product of **r**-dependent *radial functions* and θ- and φ-dependent *angular functions*. The radial function, $R_l(\kappa'\mathbf{r})$, of the deformation density takes the form of normalized Slater (or Gaussian) functions

$$R_l(\mathbf{r}) = \kappa'^3[\xi^{n_l+3}/(n_l+2)!](\kappa'\mathbf{r})^{n(l)} \exp(-\kappa'\xi_l\mathbf{r}).$$

Bader's (1990, 1998) quantum theory of *atoms in molecules* or AIM provides a pathway for comparing the experimental electron density with theoretically derived density in terms of topological properties of the density $\rho(\mathbf{r})$. The bond between any two atoms in a molecule is identified in terms of critical points, classified using the Hessian matrix of the electron density (Bader, 1990; Koch & Popelier, 1995). The line of the highest electron density linking any two atoms is referred to as the *bond path* (BP) and its length R_{ij}, which need not be the same as the inter-atomic vector, is referred to as the *interaction line*.

However, topological analysis only indicates the presence of the bond and not its character. Characterization of a bond in terms of bond order, ionicity, conjugation, hydrogen bonding and bond critical points (BCPs) becomes important in the chemical context. Koch and Popelier have proposed eight criteria for hydrogen bonding, in the AIM approach, that allow a hydrogen bond to be distinguished from a van der Waals interaction (Koch & Popelier, 1995; Popelier, 2000). Among these, the fourth criterion (mutual penetration of hydrogen and acceptor atom) is considered as *necessary and sufficient* to describe a hydrogen bond. This condition compares the non-bonded radii of the donor H atom (r_D^0) and the acceptor atom (r_A^0) with their corresponding bonding radii. The non-bonding radius is taken to be equivalent to the gas phase van der Waals radius of the participating atoms (Bondi, 1964; Nyburg & Faerman, 1985). The bonding radius (r) is the distance from the nucleus to the BCP. In a typical hydrogen bond, the value of $\Delta r_D = (r_D^0 - r_D) > \Delta r_A = (r_A^0 - r_A)$ and $\Delta r_D + \Delta r_A > 0$ represent positive interpenetration. If either or both of these conditions are violated the interaction is essentially van der Waals in nature.

2. Experimental

Colourless crystals were grown by slow evaporation at $\sim$ 281 K from a 1:1 $CHCl_3$–hexane mixture. High-resolution single-crystal X-ray diffraction data were collected, at both room temperature and low temperature, on a Bruker AXS SMART APEX CCD diffractometer using Mo $K\alpha$ radiation (50 kV, 40 mA) in Bangalore. For the low-temperature measurement, the ramp rate was set to 40 K h^{-1} to achieve the

Table 1
Experimental single-crystal X-ray diffraction data for 1-formyl-3-thiosemicarbazide at room temperature (293 K) and low temperature (100 and 90 K).

	293 K	100 K	90 K
Crystal data			
Chemical formula	$C_2H_5N_3OS$	$C_2H_5N_3OS$	$C_2H_5N_3OS$
M_r	119.16	119.15	119.16
Cell setting, space group	Monoclinic, $P2_1/c$	Monoclinic, $P2_1/c$	Monoclinic, $P2_1/c$
a, b, c (Å)	7.2569 (17), 7.4263 (18), 9.5930 (23)	7.2339 (5), 7.3703 (5), 9.4771 (7)	7.2359 (3), 7.3713 (3), 9.4768 (4)
α, β, γ (°)	90, 98.606 (4), 90	90.00, 98.4260 (10), 90.00	90, 98.403 (2), 90
V (Å^3)	511.2 (2)	499.83 (6)	500.05 (4)
Z	4	4	4
D_x (Mg m^{-3})	1.548	1.583	1.583
Radiation type	Mo $K\alpha$	Mo $K\alpha$	Mo $K\alpha$
No. of reflections for cell parameters	3850	4707	24 842
θ range (°)	2.84–26.4	2.8–26.0	2.76–50.3
μ (mm^{-1})	0.51	0.52	0.52
Temperature (K)	293 (2)	100 (2)	90 (2)
Crystal form, color	Prism, colorless	Block, colorless	Prism, colorless
Crystal size (mm)	0.37 × 0.28 × 0.16	0.28 × 0.25 × 0.16	0.37 × 0.28 × 0.16
Data collection			
Diffractometer	Bruker SMART APEX CCD area detector	CCD area detector	Bruker SMART APEX CCD area detector
Data collection method	φ and ω scans	φ and ω scans	φ and ω scans
Absorption correction	Multi-scan (based on symmetry-related measurements)	Multi-scan (based on symmetry-related measurements)	Multi-scan (based on symmetry-related measurements)
T_{min}	0.827	0.868	0.826
T_{max}	0.923	0.921	0.920
No. of measured, independent and observed reflections	3850, 1012, 961	6106, 982, 953	24 842, 5136, 4514
Criterion for observed reflections	$I > 2\sigma(I)$	$I > 2\sigma(I)$	$I > 3\sigma(I)$
R_{int}	0.014	0.017	0.025
θ_{max} (°)	26.4	26.0	50.3
Range of h, k, l	$-8 \Rightarrow h \Rightarrow 9$ $-8 \Rightarrow k \Rightarrow 9$ $-11 \Rightarrow l \Rightarrow 11$	$-8 \Rightarrow h \Rightarrow 8$ $-9 \Rightarrow k \Rightarrow 9$ $-11 \Rightarrow l \Rightarrow 11$	$-15 \Rightarrow h \Rightarrow 15$ $-15 \Rightarrow k \Rightarrow 15$ $-19 \Rightarrow l \Rightarrow 20$
Refinement			
Refinement on	F^2	F^2	F^2
$R[F^2 > 2\sigma(F^2)]$, $wR(F^2)$, S	0.029, 0.076, 1.07	0.025, 0.065, 1.08	0.014, 0.015, 1.56
No. of reflections	1012	982	4518
No. of parameters	80	80	207
H-atom treatment	Mixture of independent and constrained refinement	Mixture of independent and constrained refinement	Refined independently
Weighting scheme	$w = 1/[\sigma^2(F_o^2) + (0.0429P)^2 + 0.1699P]$, where $P = (F_o^2 + 2F_c^2)/3$	$w = 1/[\sigma^2(F_o^2) + (0.0381P)^2 + 0.2485P]$, where $P = (F_o^2 + 2F_c^2)/3$	$w^2 = 1/[\sigma^2(F_o^2)]$
$(\Delta/\sigma)_{max}$	0.001	< 0.0001	< 0.0001
$\Delta\rho_{max}$, $\Delta\rho_{min}$ (e Å^{-3})	0.24, −0.26	0.20, −0.26	0.30, −0.25

Computer programs used: Bruker *SMART* for *WNT*/2000, Version 5.629 (Bruker, 2004), Bruker *SAINT*, Version 6.45, 1997–2003 (Bruker, 2004), *SHELXS*97 (Sheldrick, 1997), Bruker *SHELXTL*, Version 6.14, 2000–2003 (Bruker, 2004), Koritsanszky *et al.* (2003), *CAMERON* (Watkin *et al.*, 1996), *PLATON* (Spek, 2001).

final temperature. During data collection the temperature was maintained at 90 (2) K with an Oxford Cryo system with N_2 flows. A suitable crystal of reasonable size (Table 1)[1] was mounted in a Lindemann capillary and allowed to stabilize at the final temperature for 1 h. Data were collected in three sets of frames with different scan times (20, 45 and 85 s) to cover the full sphere of reciprocal space with different 2θ settings of the detector (−25, −50 and −75°), and φ settings (0, 90, 180 and 270°) of the goniometer and the scanning angle ω was set to 0.3° for each of the 606 frames. An additional 60 frames were collected with 2θ settings of the detector at −25° and φ settings at 0° at the end to perform the crystal decay correction. The crystal-to-detector distance was kept at 6.07 cm. This strategy (Munshi & Guru Row, 2002, 2003) provides high resolution, large redundancy and sufficient completeness in data sets, which are the key factors for multipole refinement modeling. Data at 100 K were additionally collected in Hyderabad to provide an independent confirmation of the 90 K data because issues of tautomerism are involved. These data were also collected on a Bruker AXS SMART APEX CCD diffractometer. Both sets of collected data were monitored and reduced with the packages *SMART* (Bruker, 2004) and *SAINTPLUS* (Bruker, 2004), respectively. The charge-density analysis as described below was performed with the data collected at 90 K. Sorting, scaling, merging and empirical correction for absorption of the set of intensities were

[1] Supplementary data for this paper are available from the IUCr electronic archives (Reference: LC5030). Services for accessing these data are described at the back of the journal.

Table 2
Comparison of intra- and intermolecular interactions from 293, 100 and 90 K data *via* geometrical analysis.

For each interaction, the first, second and third rows correspond to the metrics at room temperature, 100 and 90 K, respectively.

D—H···A	D—H (Å)	H···A (Å)	D···A (Å)	D—H···A (°)
Intramolecular interaction				
N3—H3B···N5	0.84 (2)	2.39 (2)	2.703 (2)	103.8 (17)
	0.84 (2)	2.38 (2)	2.704 (2)	103.5 (12)
	0.84 (2)	2.38 (2)	2.706 (2)	103.4 (12)
Intermolecular interactions				
N3—H3A···O7	0.88 (2)	2.043 (21)	2.905 (2)	166.5 (20)
	0.87 (2)	2.030 (17)	2.882 (2)	166.9 (15)
	0.87 (2)	2.028 (15)	2.881 (2)	167.4 (14)
N5—H5···O7	0.86	2.398	2.967 (2)	124.0
	0.76 (2)	2.293 (19)	2.913 (2)	139.6 (18)
	0.80 (2)	2.260 (17)	2.909 (1)	138.8 (14)
N4—H4···S1	0.83 (2)	2.481 (20)	3.302 (2)	168.8 (18)
	0.85 (2)	2.450 (20)	3.275 (1)	167.9 (15)
	0.83 (2)	2.458 (15)	3.277 (1)	168.5 (13)
N3—H3B···S1	0.82 (2)	2.895 (20)	3.500 (2)	132.6 (17)
	0.84 (2)	2.844 (17)	3.461 (1)	131.5 (16)
	0.84 (2)	2.838 (16)	3.460 (1)	132.1 (13)
Weak interactions				
C6—H6···S1	0.97 (2)	2.970 (19)	3.591 (2)	123.1 (15)
	0.98 (2)	2.911 (19)	3.546 (1)	123.6 (13)
	0.98 (2)	2.904 (15)	3.544 (1)	124.2 (11)
N3—H3A···N4	0.88 (2)	2.827 (20)	3.400 (2)	124.1 (16)
	0.87 (2)	2.812 (16)	3.363 (2)	122.9 (14)
	0.87 (2)	2.810 (16)	3.362 (2)	122.8 (13)
C6—H6···O7	0.97 (2)	2.801 (19)	3.488 (15)	128.6 (13)
	0.98 (2)	2.753 (16)	3.439 (16)	127.8 (13)
	0.98 (2)	2.761 (16)	3.436 (14)	126.8 (15)

performed with *SORTAV* (Blessing, 1987). The structures were solved by direct methods using *SHELXS*97 (Sheldrick, 1997) and refined in the spherical atom approximation (based on F^2) by using *SHELXL*97 (Sheldrick, 1997). The crystal packing diagrams were generated from *POV-Ray* (The POV-Ray Team, 2004) using the X-Seed interface (Barbour, 2001). The thermal ellipsoid plots were obtained from *POV-Ray* (The POV-Ray team, 2004) *via ORTEP* (Johnson, 1965; Farrugia, 1997).

2.1. Multipole refinement

The multipole refinements were carried out with the module XDLSM incorporated in the *XD* package (Koritsanszky *et al.*, 2003). The function minimized in the least-squares refinement was $\sum w\left(|F_o|^2 - K|F_c|^2\right)^2$ for all reflections with $I > 3\sigma(I)$. The same refinement procedure as described earlier by some of us (Munshi & Guru Row, 2002, 2003, 2005*a*,*b*) was followed in the present study. The positions of the H atoms in this refinement as well as in the subsequent refinements were fixed to the average bond-distance values obtained from reported neutron diffraction studies (Allen, 1986; C—H 1.085, N—H 1.03 Å). Also, refinements releasing monopole, dipole, quadrupole, octupole and hexadecapole (only for the S atom) populations with single κ were performed in a stepwise manner. Finally, a single κ' parameter was refined for each species for all the non-H atoms along with the rest of the parameters (including the isotropic displacement parameters of the H atoms). Owing to the unavailability of neutron data and the absence of strong hydrogen bonds in the structure, for all H atoms the multipole expansion was truncated at the $l_{max} = 1$ (dipole, bond-directed) level. For chemically different groups of non-H atoms, separate κ and κ' parameters were allowed, while for H atoms the corresponding values were fixed at 1.2. The scale factor was allowed to refine in all the refinements.

2.2. Calculation of theoretical structure factors and atomic basin properties

The program *CRYSTAL*03 (Saunders *et al.*, 2003) was used to perform the single-point periodic calculations with the DFT method at the B3LYP level (Becke, 1993; Lee *et al.*, 1998) with a 6-31G** basis set (Hariharan & Pople, 1973). This basis set has been shown to provide reliable and consistent results with respect to studies involving intermolecular interactions (Oddershede & Larsen, 2004; Munshi & Guru Row, 2005*a*,*b*). The coordinates obtained from the final experimental multipole model were used to generate the periodic wavefunction and the theoretical static structure factors. The shrinking factors (IS1, IS2 and IS3) along the reciprocal lattice vectors were set at 4 (30 K points in the irreducible Brillouin zone).

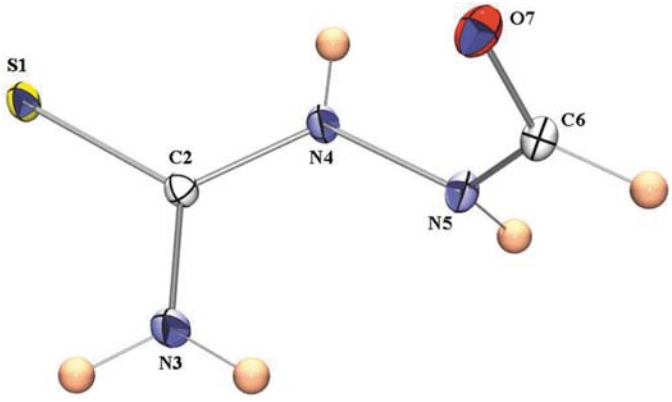

Figure 1
ORTEP (Johnson, 1965) diagram at 90 K showing atomic labeling with 50% ellipsoid probability for non-H atoms.

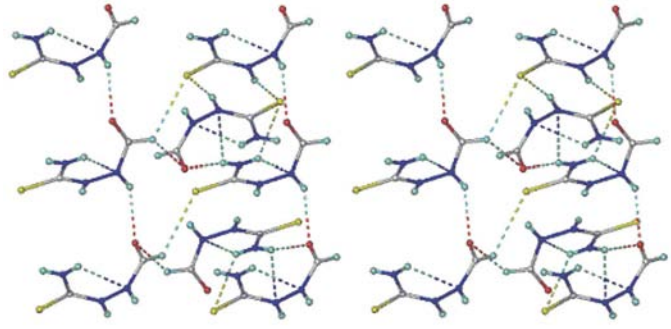

Figure 2
Stereoview of the crystal structure of 1-formyl-3-thiosemicarbazide to show all the hydrogen bonds.

The truncation parameters (ITOL), which control the accuracy of the calculation of the bielectronic Coulomb and exchange series, were set as ITOL1 = ITOL2 = ITOL3 = ITOL4 = 6 and ITOL5 = 15. Owing to the large difference between ITOL4 and ITOL5 the exponents of the polarization functions were not scaled (Spackman & Mitchell, 2001). Rapid convergence was achieved when the level shifter value was set equal to 0.5 Hartree. Upon convergence on energy ($\sim 10^{-6}$), the periodic wavefunction was obtained and used to generate the theoretical structure factors with the option XFAC. The temperature factors and atomic positions were not refined during the multipole refinement of these theoretical static structure factors *via* XD. The same multipole parameters, which were used in the refinement of experimental structure factors, were allowed to refine with separate κ' parameters for each non H-atom, including all the theoretical reflections. The module *XDPROP* of the package *XD* was used for topological analysis of the electron density.

In order to evaluate the atomic basin properties, the approach suggested earlier (Aicken & Popelier, 2000; Munshi & Guru Row, 2005*a*,*b*) using the module *TOPXD* (Volkov *et al.*, 2000) was used. *Ab initio* geometry optimization and the corresponding wavefunctions for the isolated molecule were obtained *via GAUSSIAN*98 (Frisch *et al.*, 2002) at the B3LYP level with a 6-31G** basis set and the atomic basin properties in the gas-phase for the isolated molecule was obtained from *MORPHY*98 (Popelier & Bone, 1998).

3. Results and discussion

In (I) the commonly accepted structural formula of 1-formyl-3-thiosemicarbazide is given as *A*. The tautomeric representation is given as *B*. The formula given by Saxena *et al.* (1991) who determined the crystal structure of the compound for the first time is given as *C* along with the atom-numbering scheme. We retain their atom-numbering scheme in this article. Saxena *et al.* (1991) noted that the C2—N3 bond has double-bond character, but they clearly placed two H atoms on N3 and the S atom was reported to carry a H atom. We have understood this representation to mean that there are elements of both *A* and *B* in the crystal, leaving open the possibility of an S—H···N interaction. Indeed, the configuration of the NH_2 group was reported as being out of the plane from S1—C2—N4—N5, N4 and N5 being the hydrazine N atoms. The crystal packing, as described by Saxena *et al.* (1991), consists of N—H···O hydrogen bonds formed by N3—H and N5—H. However, they did not mention the existence of any S—H···N hydrogen bond.

The structure determinations at room tempera-

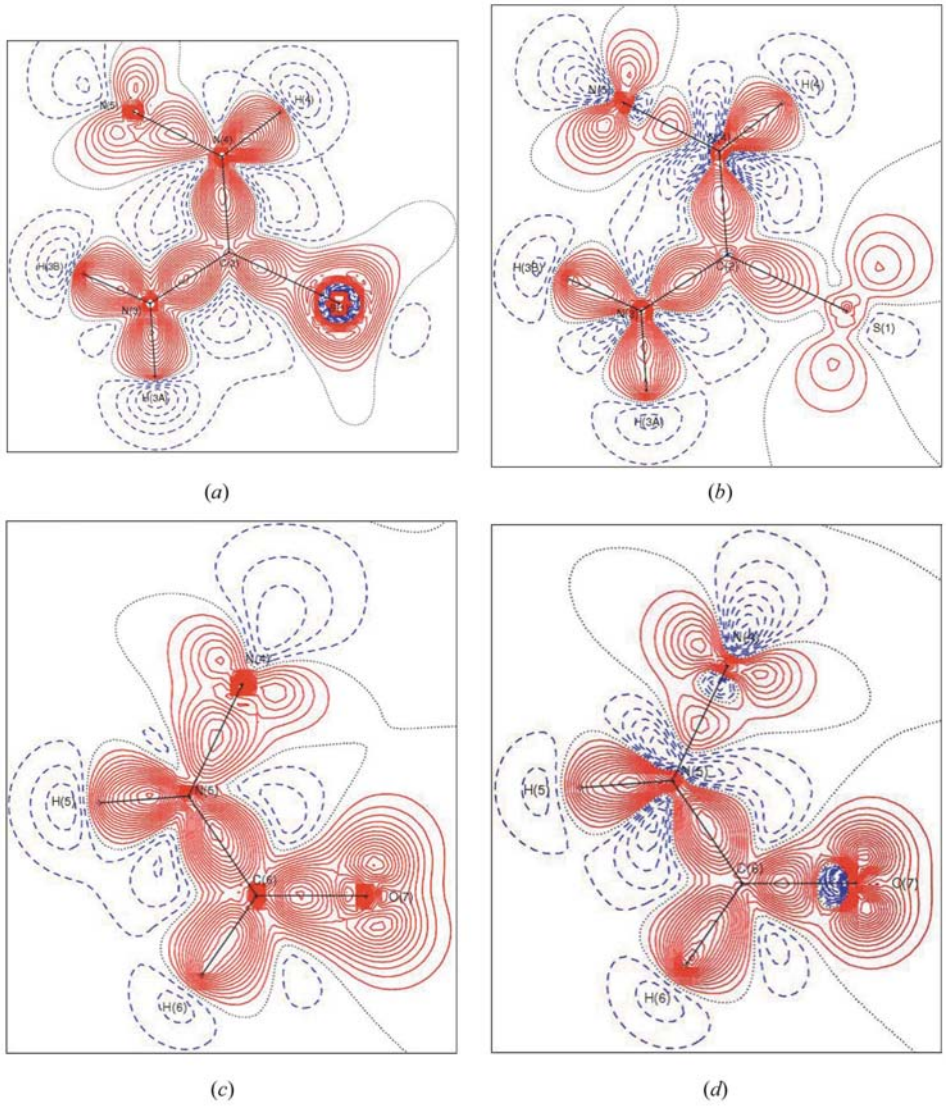

Figure 3
(*a*) Experimental static deformation electron density map in the S1—N3—N4 plane. For all static deformation density maps the positive (solid lines) and negative (broken lines) contours are with intervals of ± 0.05 e Å^{-3}. The contour at zero is shown as dotted lines. (*b*) Theoretical, static, deformation electron-density map in the S1—N3—N4 plane. (*c*) Experimental, static, deformation electron-density map in the O7—N5—N4 plane. (*d*) Theoretical, static, deformation electron-density map in the O7—N5—N4 plane.

Table 3
Intramolecular bond critical points.

The values from periodic calculation using B3LYP/6-31G** method are given in italics.

Bond ($A-B$)	ρ_b	$\nabla^2\rho_b$	R_{ij}	$d1$	$d2$	λ_1	λ_2	λ_3	ε
S1—C2	1.47 (1)	−4.74 (2)	1.7051	0.8437	0.8613	−8.42	−8.00	11.68	0.05
	1.41	*−6.75*	*1.7049*	*0.8318*	*0.8732*	*−7.44*	*−6.82*	*7.52*	*0.09*
O7—C6	2.85 (1)	−20.29 (5)	1.2275	0.8063	0.4213	−24.50	−23.44	27.64	0.05
	2.72	*−25.52*	*1.2272*	*0.7905*	*0.4368*	*−24.41*	*−21.76*	*20.65*	*0.12*
N3—C2	2.44 (1)	−30.16 (4)	1.3239	0.8382	0.4857	−20.02	−17.58	7.44	0.14
	2.37	*−26.67*	*1.3237*	*0.7994*	*0.5242*	*−19.07*	*−16.73*	*9.12*	*0.14*
N4—N5	2.38 (1)	−5.15 (3)	1.3866	0.6923	0.6943	−18.54	−18.11	31.5	0.02
	2.18	*−4.363*	*1.3861*	*0.6903*	*0.6958*	*−17.05*	*−16.43*	*29.13*	*0.04*
N4—C2	2.35 (1)	−28.04 (3)	1.3489	0.8384	0.5104	−18.78	−16.61	7.36	0.13
	2.23	*−22.79*	*1.3488*	*0.81*	*0.5388*	*−17.56*	*−15.15*	*9.92*	*0.16*
N5—C6	2.37 (1)	−26.05 (3)	1.3530	0.8321	0.5208	−18.14	−16.27	8.36	0.11
	2.30	*−25.15*	*1.3536*	*0.8129*	*0.5407*	*−18.7*	*−16.09*	*9.64*	*0.16*
N3—H3*A*	2.00 (3)	−30.63 (21)	1.0300	0.8039	0.2261	−28.8	−27.29	25.46	0.06
	1.98	*−21.64*	*1.0300*	*0.7747*	*0.2553*	*−26.08*	*−24.25*	*28.69*	*0.08*
N3—H3*B*	2.18 (4)	−27.55 (19)	1.0301	0.7683	0.2618	−28.39	−26.73	27.57	0.06
	2.02	*−20.30*	*1.0301*	*0.7586*	*0.2715*	*−25.55*	*−23.49*	*28.74*	*0.09*
N4—H4	2.02 (3)	−29.04 (22)	1.0301	0.8039	0.2263	−28.9	−26.99	26.86	0.07
	2.015	*−23.21*	*1.0300*	*0.7776*	*0.2524*	*−26.91*	*−24.78*	*28.48*	*0.09*
N5—H5	2.13 (4)	−29.07 (22)	1.0300	0.7831	0.247	−28.8	−27.2	26.93	0.06
	2.07	*−22.40*	*1.0300*	*0.7707*	*0.2594*	*−27.11*	*−24.87*	*29.58*	*0.09*
C6—H6	1.86 (3)	−19.21 (12)	1.0852	0.7442	0.341	−17.92	−17.12	15.83	0.05
	1.88	*−19.13*	*1.0850*	*0.7251*	*0.3599*	*−18.18*	*−17.21*	*16.26*	*0.06*

ture, 100 and 90 K yielded the same result, although the location of the H atoms was more straightforward in the 100 and 90 K data sets. From the data collected at room temperature, in contrast to Saxena *et al.* (1991), we found that C2—N3 is clearly a single bond while C2═S1 is indicated to be a double bond (present study, 1.696 Å; Saxena's study, 1.698 Å). The location of all the H atoms unambiguously confirms formula *A* for the compound. Again, and in contrast to Saxena *et al.* (1991), we found that the NH_2 group is coplanar with the S1—C2—N4—N5 plane. We have examined the sample for polymorphism because it is possible that we had collected data on a different tautomer. However, it was understood that the structure does not have any polymorphic character. Further, the unit cell obtained at room temperature is essentially the same as reported by Saxena *et al.* (1991). Therefore, we conclude that the analysis of Saxena *et al.* (1991) is of limited accuracy [room temperature, 946 reflections observed at the $3\sigma(I)$ level, R = 0.077] and that the possibility of an S—H···N hydrogen bond in this compound is indeed remote.

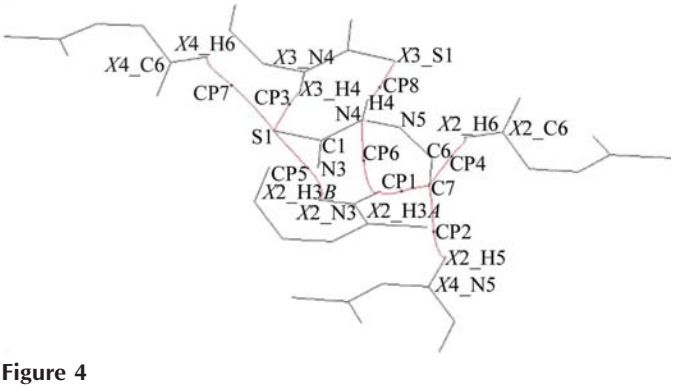

Figure 4
Bond-path character showing the critical-point locations along the interaction lines shown in red for each hydrogen bond.

1-Formyl-3-thiosemicarbazide is a small aliphatic molecule, but contains no less than five hydrogen-bond donors (two thioamide, two hydrazine, one formyl) and five acceptors (carbonyl, thiocarbonyl, thioamide, two hydrazine). Indeed, almost the entire molecular surface is decorated with hydrogen-bond donors and acceptors. Analysis of the crystal structure (present study) showed the presence of N—H···O, N—H···S, N—H···N, C—H···S and C—H···O bonds. The presence of five different varieties of hydrogen bridge (Desiraju, 2002) in the packing was considered exceptional. Furthermore, three of these are of the weaker variety (C—H···S, C—H···O and N—H···N) with the first two involving the formyl C—H group (Chaney *et al.*, 1996; Moorthy *et al.*, 2003) and the third having both intramolecular and intermolecular variations. Considering that the original question as to whether or not there is an S—H···N bridge in this crystal was essentially answered – in the negative sense – we redirected our efforts towards a charge-density study and an experimental and theoretical analysis of the many hydrogen bonds in the structure. To re-emphasize the point made above, it is indeed unusual to find so many different types of hydrogen bond in the same crystal structure, which contains not much else in terms of its supramolecular content. Notably, we wished to examine more closely the three weaker and more controversial interactions, namely N—H···N, C(formyl)—H···S and C(formyl)—H···O *via* charge-density analysis.

The unit-cell parameters, experimental details and refinement parameters, including the residual densities over the asymmetric unit, are listed in Table 1. The *ORTEP* view (90 K) in Fig. 1 shows the labeling of non-H atoms and the crystal-packing diagram is given in Fig. 2. The geometrical analysis based on the data collected at room temperature, 100 and 90 K reveals that the intramolecular N3—H3*B*···N5 interaction is noteworthy and directs the molecular conformation to bring the NH_2 group to be coplanar with the S1—C2—N4—N5 plane. All the H atoms (except H5 at room temperature, refined with the riding hydrogen option) were located from difference-Fourier maps. Interaction metrics are given in Table 2. The values at 100 and 90 K are generally similar and furnish an additional check on the measurement. Normally, a hydrogen bond becomes shorter and more linear as the temperature is lowered. Accordingly, there is no problem in assigning hydrogen-bond character to the N—H···O and N—H···S interactions. The C—H···S and C—H···O interactions, and the N—H···N interactions are weaker. Leaving out N5—H5···O7 (H atom is fixed at room

Table 4
Bonding nature between the C atom and the S atom in terms of charge-density distributions.

Compound	ρ_b	$\nabla^2\rho_b$	R_{ij}
2-Thiocoumarin[a] (C═S)	1.65 (4)	−4.56 (6)	1.6538
Present study (C→S)	1.49 (1)	−5.02 (3)	1.7048
1-Thiocoumarin[b] (C–S)	1.36 (4)	−2.08 (5)	1.7736
	1.34 (4)	−1.22 (5)	1.7472

References: (*a*) Munshi & Guru Row (2002, 2003); (*b*) Munshi & Guru Row (2005*a*).

temperature), there are small decreases in the hydrogen-bond lengths upon lowering the temperature from room temperature to 90 K (Δd for C—H···S, C—H···O and N—H···N are 0.066, 0.040 and 0.017 Å, respectively; Table 2). However, the hydrogen-bond angles decrease upon such lowering for N3—H3*A*···N4 ($\Delta\theta = -1.3$) and C—H···O (−1.8), suggesting that these interactions are marginal at best. At this stage, a detailed analysis of the charge-density distribution was carried out to investigate the nature of the above-mentioned interactions.

3.1. Charge-density analysis of the 90 K data set

In the final refinement, Hirshfeld's rigid-bond test (Hirshfeld, 1976) was verified and the value of the maximum differences of the mean-square displacement amplitudes was found to be 4×10^{-4} Å^2 for the bonds S1—C2 and N4—C2, indicating that the atomic thermal vibrations are properly accounted for. It is generally observed that the description of the charge-density distribution in the vicinity of the S atom appears to be difficult (Overgaard & Hibbs, 2004). In their study Espinosa *et al.* (1997) have shown that the use of different sets of parameters of the Slater-type sulfur radial function can improve the multipolar model. However, no such analysis was performed in our present study, but after several trials with different refinement strategies the present multipole model was picked to be the best for the remaining analyses. The residual density maps (see supplementary material, Fig. S1) in the plane of the molecule obtained from the final multipole model are almost featureless, indicating the accuracy of the electron density model. The minimum (−0.25 e Å^{-3}) and maximum (+0.30 e Å^{-3}) residual densities (Table 1) over the entire asymmetric unit were found mainly near the S atom (Fig. S1*a*). It is noteworthy that the residuals in the vicinity of the next heaviest atom, O, are almost negligible (±0.16 e Å^{-3}). The corresponding dynamic deformation-density maps (Fig. S2) show the deformation of valence electron densities in the bonding region and the lone pair of electrons. The static maps (excluding atomic thermal vibrations) obtained from the multipole analysis of both experimental and theoretical structure factors show almost similar features (Figs. 3*a*–*d*). The lone pair of electrons on the S atom (Figs.

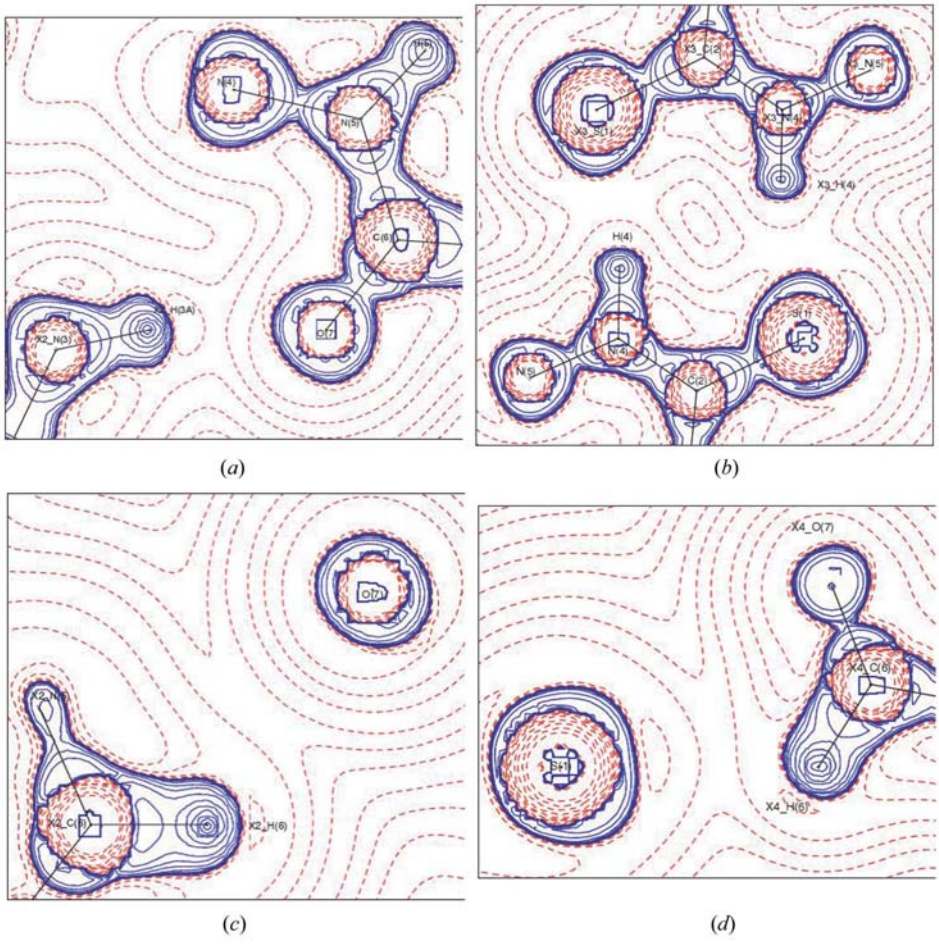

Figure 5
(*a*) Laplacian [$\nabla^2\rho_b(\mathbf{r})$] distribution of a representative N—H···O hydrogen bond. All the Laplacian maps are drawn at logarithmic intervals in $-\nabla^2\rho_b$ e Å^{-5}, solid and broken lines represent positive and negative contours, respectively. (*b*) Laplacian [$\nabla^2\rho_b(\mathbf{r})$] distribution of N—H···S hydrogen bonds showing the formation of the dimer. (*c*) Laplacian [$\nabla^2\rho_b(\mathbf{r})$] distribution of the C—H···O hydrogen bond. (*d*) Laplacian [$\nabla^2\rho_b(\mathbf{r})$] distribution of the C—H···S hydrogen bond.

Table 5
Intermolecular bond-critical points and the parameters characterizing the interactions along with the curvatures, the values from periodic calculation using B3LYP/6-31G** method are given in italics.

Interaction	$\Delta r_D - \Delta r_A$	$\Delta r_D + \Delta r_A$	R_{ij}	ρ_b	$\nabla^2\rho_b$	$G(r_{CP})$	$V(r_{CP})$	$E(r_{CP})$	λ_1	λ_2	λ_3
N3—H3*A*···O7^{i}	0.297	0.863	1.876	0.14	3.42	74.5	−55.8	18.7	−0.71	−0.68	4.81
	0.198	*0.866*	*1.874*	*0.17*	*3.21*	*73.9*	*−60.5*	*13.4*	*−0.83*	*−0.83*	*4.87*
N5—H5···O7^{ii}	0.145	0.606	2.134	0.11	1.93	43.00	−33.5	9.5	−0.50	−0.47	2.90
	0.117	*0.628*	*2.112*	*0.12*	*1.97*	*44.6*	*−35.4*	*9.2*	*−0.50*	*−0.49*	*2.97*
N4—H4···S1^{iii}	0.291	0.673	2.268	0.11	1.85	41.2	−31.9	9.3	−0.42	−0.36	2.64
	0.304	*0.676*	*2.264*	*0.15*	*2.02*	*49.1*	*−43.3*	*5.8*	*−0.57*	*−0.53*	*3.11*
N3—H3*B*···S1^{iv}	0.136	0.200	2.74	0.05	0.73	15.1	−10.4	4.7	−0.18	−0.11	1.02
	0.209	*0.242*	*2.698*	*0.07*	*0.86*	*19.0*	*−14.6*	*4.4*	*−0.20*	*−0.17*	*1.23*
N3—H3*A*···N4^{iv}	0.115	0.035	2.765	0.04	0.62	12.9	−8.7	4.1	−0.11	−0.10	0.83
	0.096	*0.038*	*2.762*	*0.04*	*0.66*	*13.6*	*−9.4*	*4.2*	*−0.11*	*−0.08*	*0.84*
C6—H6···O7^{ii}	0.025	0.030	2.71	0.03	0.50	10.1	−6.6	3.5	−0.12	−0.08	0.70
	0.062	*0.014*	*2.726*	*0.04*	*0.55*	*11.2*	*−7.4*	*3.8*	*−0.12*	*−0.09*	*0.77*
C6—H6···S1^{v}	0.040	0.087	2.853	0.05	0.61	13.2	−9.9	3.3	−0.16	−0.14	0.91
	0.117	*0.082*	*2.858*	*0.05*	*0.64*	*13.9*	*−10.4*	*3.4*	*−0.17*	*−0.14*	0.94

Symmetry codes: (i) $-x+1, y+\frac{1}{2}, z+\frac{3}{2}$; (ii) $-x+2, y+\frac{1}{2}, -z+\frac{3}{2}$; (iii) $-x+1, -y+2, -z+1$; (iv) $-x+1, y+\frac{1}{2}, -z+\frac{3}{2}$; (v) $x-1, -y+\frac{3}{2}, z-\frac{1}{2}$.

3*a*) and the O atom (Fig. 3*b*) is prominently seen in both maps. However, a depletion of charge density along the C2—S1 and N4—N5 bonds is observed in the theoretical map compared with the experimental map (Fig. 3*a*).

Table 3 lists the experimental topological parameters of the covalent bonds within the molecule along with the values obtained from periodic theoretical calculations. Comparison of experimental and theoretical values led to the following observations. The values of $\rho_b(\mathbf{r})$ from experiment are higher in magnitude, with the highest difference being 0.2 e Å^{-3} only for the N5—C6 bond. The highest electron density was found at the C═O bond and that of the lowest at the C═S bond and the Laplacian values obtained from experiment and theory are comparable for each bond. The values of R_{ij} are in excellent agreement and the location of the BCPs for the bonds are found to be lying away from the first atom, as listed in Table 3, except for the C═S and N—N bonds, where it is almost at the center. The values of bond ellipticity, ε, are also comparable for each bond and they are almost cylindrical in nature. These observations indicate that both experimental and theoretical methodologies provide reasonable comparative measures of the topological and charge-density properties. It is interesting to note that the C═S bond shows partial double-bond nature in terms of $\rho_b(\mathbf{r})$ and R_{ij} compared with the values reported earlier (Munshi & Guru Row, 2002, 2003, 2005*a*,*b*) from charge-density studies at 90 K. This observation indicates that there is a possible resonance among the bonds (Table 4).

Table 5 lists the intermolecular interactions based on the first four of Koch and Popelier's criteria. Further, based on Koch and Popelier's important fourth criterion, the values of $(\Delta r_D + \Delta r_A) > 0$ and $(\Delta r_D - \Delta r_A) > 0$ from both experiment and theory suggest that *all the observed interactions are hydrogen bonds* rather than van der Waals interactions. Among these, the N—H···O hydrogen bonds [R_{ij} = 1.88, 2.13 Å; $E(r_{CP})$ = 18.7, 9.5 kJ mol^{-1} bohr^{-3}] are the strongest, particularly in terms of the total energy density, followed by N—H···S, N—H···N, C—H···O and C—H···S (Table 5). These observations are in agreement with the experimental study (Espinosa *et al.*, 1998; Espinosa & Molins, 2000) of a set of 83 *X*—H···O hydrogen bonds (*X* = C, N, O). However, one can also compare the strength of different H···*X* (*X* = O, N, S) interactions based on the normalization of *E* by ρ (E/ρ, called *the bond degree parameter*), which gives the total energy per electron at a bond critical point (Espinosa *et al.*, 2002). The lowest ρ_b value (0.03 e Å^{-3}) was found for the C—H···O hydrogen bond, as expected. The magnitudes of all three curvatures are found to be higher in the case of stronger hydrogen bonds and the values obtained from experiment and theory are comparable (Table 5). The bond-path characteristics and the corresponding Laplacian maps from experimental analysis (Figs. 4 and 5) provide further insights into the bonding features. The corresponding theoretical maps are not shown in the figure since they display similar features. Fig. 4 traces the location of BCPs along with the BPs for all hydrogen bonds in the structure. The O atom is trifurcated with two strong N—H···O and one weak C—H···O hydrogen bonds, while the S atom is trifurcated *via* two N—H···S and one C—H···S hydrogen bonds. There is only one intermolecular N—H···N hydrogen bond directed towards the lone pair of the N atom (Fig. 5*a*), along with one of the N—H···O hydrogen bonds. One of the N—H···S hydrogen bonds generates a dimer across a centre of symmetry (Fig. 4) and the corresponding electron-density distributions in this region are shown in Fig. 5(*b*). The Laplacian maps in the region of C—H···O (Fig. 5*c*) and C—H···S (Fig. 5*d*) show that the directionality of the interactions is towards the lone pair of electrons of the O atom and S atom, respectively. The multipole population parameters ($P_{lm\pm}$ and P_v) along with κ and κ' from experimental and theoretical refinements, the values of exponents of the radial function, the residual electron density maps and dynamic deformation density maps are provided as supplementary material.

The integrated properties of the H atoms involved in the hydrogen bonding were evaluated to verify the remaining Koch–Popelier criteria. These properties include the determination of the charge, potential energy, dipolar polarization

Table 6

(*a*) Atomic net charges (*q*) of the H atoms in the crystal and in the isolated molecule and their corresponding differences (in a.u.).

		q (crystal)		*q* (isolated)	Δ*q* (crystal − isolated)	
Interactions	Atom	Expt. (*E*)	Theo. (*T*)	DFT	*E*-DFT	*T*-DFT
N3—H3*A*···O7	H3*A*	0.6279	0.4625	0.4587	0.0998	0.0038
N3—H3*A*···N4						
N3—H3*B*···S1	H3*B*	0.509	0.4153	0.4355	0.0311	−0.0202
N4—H4···S1	H4	0.554	0.4578	0.4573	0.1293	0.0005
N5—H5···O7	H5	0.5312	0.4362	0.4219	0.0783	0.0143
C6—H6···O7	H6	0.1854	0.1119	0.0204	0.1639	0.0915
C6—H6···S1						

(*b*) Atomic potential energy (*PE*) of the H atoms in the crystal and in the isolated molecule and their corresponding differences (in a.u.).

		PE (crystal)		*PE* (isolated)	Δ*PE* (crystal − isolated)	
Interactions	Atom	Expt. (*E*)	Theo. (*T*)	DFT	*E*-DFT	*T*-DFT
N3—H3*A*···O7	H3*A*	−0.6403	−0.8333	−0.8552	0.2149	0.0219
N3—H3*A*···N4						
N3—H3*B*···S1	H3*B*	−0.811	−0.8935	−0.8797	0.0687	−0.0138
N4—H4···S1	H4	−0.7228	−0.8328	−0.8591	0.1363	0.0263
N5—H5···O7	H5	−0.7778	−0.8737	−0.9007	0.1229	0.0270
C6—H6···O7	H6	−1.0798	−1.1827	−1.2307	0.1509	0.0480
C6—H6···S1						

(*c*) Atomic dipolar polarization (*M*) of the H atoms in the crystal and in the isolated molecule and their corresponding differences (in a.u.).

		M (crystal)		*M* (isolated)	Δ*M* (crystal − isolated)	
Interactions	Atom	Expt. (*E*)	Theo. (*T*)	DFT	*E*-DFT	*T*-DFT
N3—H3*A*···O7	H3*A*	0.087	0.1254	0.1687	−0.0817	−0.0433
N3—H3*A*···N4						
N3—H3*B*···S1	H3*B*	0.0828	0.1307	0.1738	−0.091	−0.0431
N4—H4···S1	H4	0.1227	0.1367	0.1716	−0.0489	−0.0349
N5—H5···O7	H5	0.0926	0.1331	0.1761	−0.0835	−0.0430
C6—H6···O7	H6	0.1427	0.0944	0.1401	0.0026	−0.0457
C6—H6···S1						

(*d*) Atomic volume (*V*) of the H atoms in the crystal and in the isolated molecule and their corresponding differences (in a.u.).

		V (crystal)		*V* (isolated)	Δ*V* (crystal − isolated)	
Interactions	Atom	Expt. (*E*)	Theo. (*T*)	DFT	*E*-DFT	*T*-DFT
N3—H3*A*···O7	H3*A*	12.75	19.17	27.21	−14.46	−8.04
N3—H3*A*···N4						
N3—H3*B*···S1	H3*B*	18.43	24.86	26.56	−8.13	−1.70
N4—H4···S1	H4	18.04	20.57	27.57	−9.53	−7.00
N5—H5···O7	H5	17.50	22.65	29.12	−11.62	−6.47
C6—H6···O7	H6	41.57	40.27	50.30	−8.73	−10.03
C6—H6···S1						

and volume of H atoms, considering the crystal (experimental and theoretical) and the isolated molecule. It is to be noted that all the H atoms present in the structure participate in at least one interaction. Table 6 provides the detail of these properties for all the hydrogen bonds. The atomic Δ*q* values in the interaction region show the expected trend of increasing net charge [except H(3*B*), from theory] of the interacting H atoms in the crystal (Table 6*a*). The corresponding values of Δ*PE* also show a similar trend of increasing atomic potential energy (Table 6*b*). The decrease of atomic dipolar polarization, Δ*M*, and the depletion of atomic volume, Δ*V*, of the H atoms are evident from Tables 6(*c*) and (*d*), respectively. These values clearly bring out the quantitative features of the hydrogen bonds in the crystal.

A significant enhancement of the experimental [8.9 (4) D] and theoretical [7.2 D] molecular dipole moments in the crystal was observed when compared with the results from the single molecule, optimized geometry calculation (6.4 D). The rather high estimate of the dipole moment from the experimental charge density is to be expected based on the observations made in the charge density analysis of 2-methyl-4-nitroaniline (Howard *et al.*, 1991). Recently, careful evaluation

of molecular dipole moments from the multipole refinement of X-ray diffraction data has emphasized the influence of the crystal lattice on the enhancement of molecular dipole moments (Gatti *et al.*, 1994; May *et al.*, 2001, and references therein; Arnold *et al.*, 2000).

4. Conclusions

An accurate X-ray structure analysis rules out the possibility of an S—H···N interaction in 1-formyl-3-thiosemicarbazide. Both geometrical and charge-density analysis reveal the presence of five different varieties of hydrogen bonds in the crystal packing. From quantitative analysis of all the intermolecular interactions using the 'atoms in molecules' approach and the Koch–Popelier criteria it was found that the N—H···O interaction is strongest among five followed by N—H···S, N—H···N, C—H···O and C—H···S in order of decreasing hydrogen bond strengths (total energy densities). The systematic use of Koch–Popelier criteria to determine the nature of hydrogen bonds based on high-resolution, low-temperature X-ray diffraction data together with theoretical calculations thus provide an unique platform to obtain insights into intermolecular interactions.

PM and TST thanks CSIR and UGC for research fellowships. TNG thanks the DST for grant DST0463. GRD thanks DST and DRDO for ongoing support. We thank DST-IRHPA, India, for the CCD facilities at Bangalore (IISc) and Hyderabad (UH).

References

Aicken, F. M. & Popelier, P. L. A. (2000). *Can. J. Chem.* **78**, 415–426.
Allen, F. H. (1986). *Acta Cryst.* B**42**, 515–522.
Allen, F. H. (2002). *Acta Cryst.* B**58**, 380–388.
Allen, F. H. & Motherwell, W. D. S. (2002). *Acta Cryst.* B**58**, 407–422.
Ambalalavanan, P., Palani, K., Ponnuswamy, M. N., Thirumuruhan, R. A., Yathirajan, H. S., Prabhuswamy, B., Raju, C. R., Nagaraja, P. & Mohana, K. N. (2003). *Mol. Cryst. Liq. Cryst. Sci. Technol. Sect. A*, **393**, 63–73.
Arnold, W. D., Sanders, L. K., McMahon, M. T., Volkov, A. V., Wu, G., Coppens, P., Wilson, S. R., Godbout, N. & Oldfield, E. (2000). *J. Am. Chem. Soc.* **122**, 4708–4717.
Bader, R. F. W. (1990). *Atoms in Molecules – A Quantum Theory*. Oxford: Clarendon Press.
Bader, R. F. W. (1998). *J. Phys. Chem. A*, **102**, 7314–7323.
Barbour, L. J. (2001). *J. Supramol. Chem.* **1**, 189–191.
Bats, J. W. (1976). *Acta Cryst.* B**32**, 2866–2870.
Becke, A. D. (1993). *J. Chem. Phys.* **98**, 5648–5652.
Blessing, R. H. (1987). *Crystallogr. Rev.* **1**, 3–58.
Bondi, A. (1964). *J. Phys. Chem.* **68**, 441–451.
Bruker (2004). *SMART* (Version 5.628) and *SAINT* (Version 6.45*a*). Bruker AXS Inc., Madison, Wisconsin, USA.
Chaney, J. D., Goss, C. R., Folting, K., Santarsiero, B. D. & Hollingsworth, M. D. (1996). *J. Am. Chem. Soc.* **118**, 9432–9433.
Coppens, P. (1997). *X-ray Charge Densities and Chemical Bonding*. New York: Oxford University Press.
Coppens, P. (1998). *Acta Cryst.* A**54**, 779–788.
Desiraju, G. R. (2002). *Acc. Chem. Res.* **35**, 565–573.
Desiraju, G. R. & Steiner, T. (1999). *The Weak Hydrogen Bond in Structural Chemistry and Biology*, pp. 253–266. Oxford University Press.
Espinosa, E., Alkorta, I., Elugero, J. & Molins, E. (2002). *J. Chem. Phys.* **117**, 5529–5542.
Espinosa, E. & Molins, E. (2000). *J. Chem. Phys.* **113**, 5686–5694.
Espinosa, E., Molins, E. & Lecomte, C. (1997). *Phys. Rev. E*, **56**, 1820–1833.
Espinosa, E., Molins, E. & Lecomte, C. (1998). *Chem. Phys. Lett.* **285**, 170–173.
Farrugia, L. J. (1997). *J. Appl. Cryst.* **30**, 565.
Frisch, M. J. *et al.* (2002). *Gaussian*98, Revision A.11.3. Gaussian, Inc., Pittsburgh, PA.
Gatti, C., Saunders, V. R. & Roetti, C. (1994). *J. Chem. Phys.* **101**, 10686–10696.
Hansen, N. K. & Coppens, P. (1978). *Acta Cryst.* A**34**, 909–921.
Hariharan, P. C. & Pople, J. A. (1973). *Theor. Chim. Acta*, **28**, 213–222.
Hirshfeld, F. L. (1976). *Acta Cryst.* A**32**, 239–244.
Howard, S. T., Hursthouse, M. B., Lehmann, C. W., Mallinson, P. R. & Frampton, C. S. (1991). *J. Chem. Phys.* **97**, 5616–5630.
Jetti, R. K. R., Boese, R., Thakur, T. S., Vangala, V. R. & Desiraju, G. R. (2004). *Chem. Commun.* pp. 2526–2527.
Johnson, C. K. (1965). *ORTEP*. Report ORNL-3794. Oak Ridge National Laboratory, Tennessee.
Koch, U. & Popelier, P. L. A. (1995). *J. Phys. Chem.* **99**, 9747–9754.
Koritsanszky, T. S. & Coppens, P. (2001). *Chem. Rev.* **101**, 1583–1621.
Koritsanszky, T. S., Howard, S., Macchi, P., Gatti, C., Farrugia, L. J., Mallinson, P. R., Volkov, A., Su, Z., Richter, T. & Hansen, N. K. (2003). *XD*, Version 4.10, July. Free University of Berlin, Germany, University of Wales, Cardiff, UK, Università di Milano, Italy, CNR-ISTM, Milano, Italy, University of Glasgow, Scotland, State University of New York, Buffalo, USA, University of Nancy, France.
Lee, C., Yang, W. & Parr, R. G. (1998). *Phys. Rev. B*, **37**, 785–789.
May, E., Destro, R. & Gatti, C. (2001) *J. Am. Chem. Soc.* **123**, 12248–12254.
Moorthy, J. N., Venkatakrishnan, P., Mal, P., Dixit, S. & Venugopalan, P. (2003). *Cryst. Growth Des.* **3**, 581–585.
Munshi, P. & Guru Row, T. N. (2002). *Acta Cryst.* B**58**, 1011–1017.
Munshi, P. & Guru Row, T. N. (2003). *Acta Cryst.* B**59**, 159.
Munshi, P. & Guru Row, T. N. (2005*a*). *J. Phys. Chem. A*, **109**, 659–672.
Munshi, P. & Guru Row, T. N. (2005*b*). *Cryst. Rev.* **11**, 199–241.
Nyburg, S. C. & Faerman, C. H. (1985). *Acta Cryst.* B**41**, 274–279.
Oddershede, J. & Larsen, S. (2004). *J. Phys. Chem. A*, **108**, 1057–1063.
Overgaard, J. & Hibbs, D. E. (2004). *Acta Cryst.* A**60**, 480–487.
Popelier, P. L. A. (2000). *Atoms in Molecules. An Introduction*, pp. 150–153. England: Prentice Hall.
Popelier, P. L. A. & Bone, R. G. A. (1998). *MORPHY*98. UMIST, Manchester, England.
Saunders, V. R., Dovesi, R., Roetti, C., Causa, M., Harrison, N. M., Orlando, R. & Zicovich-Wilson, C. M. (2003). *CRYSTAL*03 1.0 *User's Manual.* University of Torino, Italy.
Saxena, A. K., Sinha, S. K. & Singh, T. P. (1991). *Acta Cryst.* C**47**, 2374–2376.
Sheldrick, G. M. (1997). *SHELXS*97 and *SHELXL*97. University of Göttingen, Germany.
Spackman, M. A. & Mitchell, A. M. (2001). *Phys. Chem. Chem. Phys.* **3**, 1518–1523.
Spek, A. L. (2001). *PLATON*. Utrecht University, The Netherlands.
The POV-Ray Team (2004). *POV-Ray for Windows.* Persistence of Vision Raytracer Pty. Ltd, PO Box 407, Williamstown, Victoria 3016 Australia. (http://www.povray.org)
Volkov, A., Gatti, C., Abramov, Yu. & Coppens, P. (2000). *Acta Cryst.* A**56**, 252–258.
Watkin, D. J., Prout, C. K. & Pearce, L. (1996). *CAMERON*. Chemical Crystallography Laboratory, University of Oxford, England.
Zhu-Ohlbach, Q., Gleiter, R., Rominger, F., Schmidt, H. L. & Reda, T. (1998). *Eur. J. Org. Chem.* pp. 2409–2416.